Accepted Manuscript

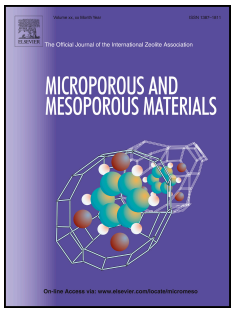

High Resolution Transmission Electron Microscopy: A Key Tool to Understand Drug Release from Mesoporous Matrices

Marina Martínez-Carmona, Montserrat Colilla, M. Luisa Ruiz-González, José M. González-Calbet, María Vallet-Regí

PII: S1387-1811(16)00029-9

DOI: 10.1016/j.micromeso.2016.01.019

Reference: MICMAT 7531

To appear in: *Microporous and Mesoporous Materials*

Received Date: 29 September 2015

Revised Date: 8 January 2016

Accepted Date: 13 January 2016

Please cite this article as: M. Martínez-Carmona, M. Colilla, M.L. Ruiz-González, J.M. González-Calbet, M. Vallet-Regí, High Resolution Transmission Electron Microscopy: A Key Tool to Understand Drug Release from Mesoporous Matrices, *Microporous and Mesoporous Materials* (2016), doi: 10.1016/j.micromeso.2016.01.019.

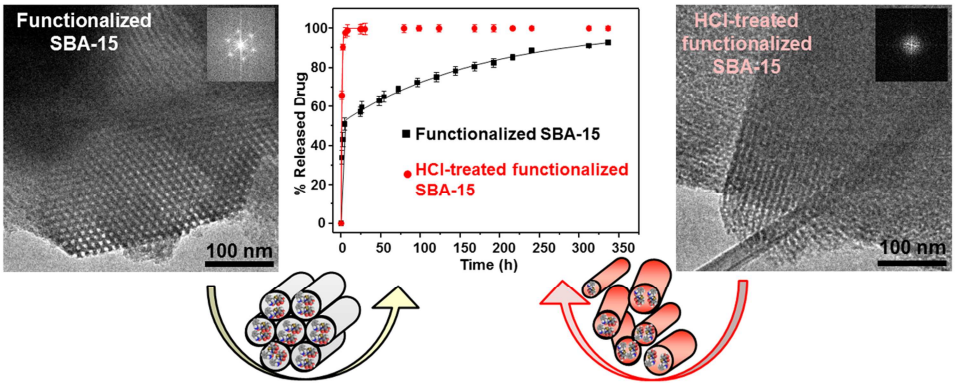

Revised Manuscript submitted to

Microporous and Mesoporous Materials

on January 2016

High Resolution Transmission Electron Microscopy: A Key Tool to Understand Drug Release from Mesoporous Matrices

Marina Martínez-Carmona,[1,2,4] Montserrat Colilla,[1,2,4,*] M. Luisa Ruiz-González,[3,4] José M. González-Calbet[3,4] and María Vallet-Regí. [1,2,4]*

[1] Departamento de Química Inorgánica y Bioinorgánica. Facultad de Farmacia, Universidad Complutense de Madrid. Instituto de Investigación Sanitaria Hospital 12 de Octubre i+12. Plaza Ramón y Cajal s/n, E-28040 Madrid, Spain.

[2] Center on Bioengineering, Biomaterials and Nanomedicine (CIBER-BBN), Spain

[3] Departamento de Química Inorgánica, Facultad de Químicas, UCM, Spain.

[4] CEI Campus Moncloa, UCM-UPM, Madrid, Spain.

* Corresponding authors. E-mail addresses: vallet@ucm.es, mcolilla@ucm.es

Phone: +34913941861 Fax: +34 394 17 86

Abstract

This work demonstrates that high resolution transmission electron microscopy (HRTEM) is an essential tool to understand drug delivery performance of mesoporous silica materials, mainly those submitted to functionalization processes involving harsh conditions that may affect the mesostructure. Herein a SBA-15-type mesoporous material bearing $\equiv Si(CH_2)_2P(O)(OCH_2CH_3)_2$ groups was synthetized following the co-condensation route. Then, the resulting material was treated with 37% wt. HCl to convert ethylphosphonate groups to ethylphosphonic acid groups. The proper dealkylation of ethoxy groups following acid treatment was confirmed by FTIR and CP-MAS $^{1}H \rightarrow {}^{13}C$ solid state NMR, which indicated the presence of $\equiv Si(CH_2)_2P(O)(OH)_2$ functionalities in the treated sample. Characterization of mesoporous materials by XRD diffraction and N_2 adsorption points to well-ordered SBA-15 structures in both untreated and acid-treated samples. Nonetheless, a deep study by HRTEM reveals that the acid-treatment provokes noticeable loss of mesostructural order, only remaining small crystalline domains. This structural damage does not influence cargo loading but it severely affects the release of molecules confined into the mesopores, as concluded from *in vitro* delivery tests using cephalexin as model drug. Thus, whereas untreated sample showed a sustained diffusion-controlled drug release during more than 2 weeks, 100% of the loaded drug was released only after 10 hours from treated sample. This abrupt burst effect cannot be explained on the basis of the existing matrix-drug interactions, whose nature and extension is quite similar under the release conditions for both samples. Thus, it can be only understood on the basis of the mesostructural damage revealed by HRTEM studies.

Keywords: Silica-based mesoporous materials, functionalization, mesostructural order, high resolution transmission electron microscopy, drug delivery.

1. Introduction

Since silica-based ordered mesoporous materials entered the drug delivery landscape back in 2001,[1] they have received growing attention by the scientific community.[2-14] Mesoporous silicas are attractive drug carriers due to their outstanding properties, including: *i) low toxicity and biocompatibility*; *ii)* an *ordered pore arrangement*, with narrow pore size distributions that allow controlling drug loading and release kinetics; *iii) high surface area*, that provides high potential for drug adsorption; *iv) great pore volume* to house high amount of therapeutic molecules; *v)* a *silanol-containing surface*, which can be functionalized to achieve higher control over drug loading and release.

Understanding drug delivery profiles from mesoporous matrices is essential to exploit their potential as controlled release systems. Drug release process obey four sequential steps:[15] penetration of the release medium into the pore network, which is governed by osmotic pressure derived from concentration gradients; drug dissolution in the release medium; drug diffusion through the porous cavities due to concentration gradients; and drug diffusion and convection within the delivery medium. The structural and textural properties of mesoporous materials together with the chemical nature of their surface are the driving factors that govern the release of molecules and determine drug delivery profiles.[2,5] Thus, pore diameter is a limiting factor for the diffusion of the molecules to the delivery medium, thus regulating the release rate.[1,16] Pore connectivity and structure also influence drug release kinetics. [17,18,20] For instance 3D-bicontinuous cubic mesostructures allow easy fluid accessibility and fast molecular transport than 2D-hexagonal array of pores.[17] However, organic modification or functionalization of mesoporous matrices is cornerstone in the performance of these materials as drug delivery systems.[2,5,19,20] Commonly, functionalization strategies of mesoporous silicas rely on the covalently grafting of organic silanes ($(RO)_3SiR'$).[21]

This process permits the modification of the silica surface by grafting organic groups selective to the chemical nature of the drug to be hosted. In most cases, organic modification allows increasing host-guest interaction between the mesoporous matrix and the drug molecule. Matrix-drug interactions are usually established through electrostatic or Coulombic interaction, hydrogen bonding, and apolar interaction,[5,22,23] offering many possibilities to control drug adsorption and release. Some functionalization processes require post-synthesis treatments under rather harsh conditions, highlighting those involving strong acids, which could affect the mesostructural order.[24] For instance, the treatment of SBA-15 functionalized with –CN groups followed by treatment with 48 % wt. H_2SO_4 to oxidize cyanide groups to carboxylic acid groups (–COOH);[25,26] or the treatment of SBA-15 functionalized with $–P(O)(OCH_2CH_3)_2$ groups followed by the treatment with 37% wt. HCl to dealkylate phosphonate groups to phosphonic acid groups ($–P(O)(OH)_2$).[27] Whatever the functionalization method used to organically modify the surface of mesoporous matrices, but highlighting those involving aggressive conditions, it is indispensable to deeply study the properties of the resulting materials by using suitable characterization techniques. Actually, any alteration in the mesostructural order could strongly influence drug release process leading to unforeseen delivery profiles, albeit, to the best of our knowledge, this has not been reported yet.

Herein we demonstrate that high resolution transmission electron microscopy (HRTEM) is an essential tool to understand drug release kinetics from mesoporous matrices. For this purpose, SBA-15 incorporating ethylphosphonate functions ($–(CH_2)_2P(O)(OH)_2$) was synthetized by co-condensation route and then was treated with concentrated HCl under reflux to achieve ethylphosphonic acid moieties ($–(CH_2)_2P(O)(OH)_2$). Although X-ray diffraction (XRD) and N_2 adsorption studies point

to well-ordered 2D-hexagonal structures in both samples, *in vitro* drug delivery profiles are dramatically different, despite of exhibiting similar host-guest interactions under the release conditions. This behavior can be only explained if a deep characterization of samples by HRTEM is performed. Such study reveals that there is a noticeable loss of mesostructure in acid-treated sample, which would account for the rapid and uncontrolled drug release kinetics.

2. Materials and methods

2.1. Synthesis of Materials

SBA-15 type mesoporous silica material containing nominal 15 mol% (based on silicon) phosphonic acid diethyl ester groups ($SBA15_{DPT}$) was synthetized by the co-condensation route using diethylphosphatoethyltriethoxysilane (DPT, 92%, ABCR) (Scheme 1). Briefly, 8.0 g of Pluronic® P123 block copolymer ($PEO_{20}PPO_{70}PEO_{20}$) kindly provided by BASF Co.) was added to a mixture of 276 mL of H_2O and 20.6 mL of concentrated HCl (37% wt., Aldrich).[28] The solution was moderately stirred at 35 ºC until total surfactant dissolution. Then, 14.1 mL of tetraethyl orthosilicate (TEOS, 98% wt., Aldrich) was added. After *ca.* 20 min a white powder appeared. Then, 3.6 mL of DPT previously dissolved in 18 mL of isopropanol (C_3H_7OH, 99.5% wt, Aldrich) was dropwise added to the suspension. The molar composition of the reaction mixture was: 0.85 TEOS: 0.15 DPT: 0.017 P123: 3.4 HCl: 208 H_2O: 3.4 C_3H_7OH. Mixtures were kept under magnetic stirring at 35ºC for 24 h and then sealed in glass beakers and heated at 100 ºC for further 24 h. Then, the obtained products were filtered, washed with deionized water, and then dried at 60ºC for 24 h. Finally, the surfactant was removed by a previously reported solvent extraction method.[29] Briefly, 1 g of

material was soaked into a beaker containing 100 mL of an isooctane-ethanol (3 : 2) mixture (isooctane, ≥99.5% wt, Aldrich; ethanol, 95%, Panreac) and kept under magnetic stirring at room temperature for 48 h. Afterward, the sample was filtered and then subjected to a second extraction process by soaking the powder into 120 mL of an acetone-water (1 : 1) mixture (acetone, QP, Panreac) for 24 h at room temperature under magnetic stirring. After the extraction processes samples were left to dry in a vacuum oven at 40ºC for 24 h to ensure total solvent removal.

Phosphonate ester groups can be transformed readily to phosphonic acid groups by acid-catalyzed hydrolytic dealkylation in concentrated HCl. Thus, SBA-15 type mesoporous silica material containing nominal 15% mol% (based on silicon) phosphonic acid groups (HCl-SBA15$_{DPT}$) was obtained from SBA15$_{DPT}$ by using a previously reported procedure consisting on treating the SBA15DPT sample with concentrated HCl (Scheme 1).[27] Briefly, 0.5 g of SBA15$_{DPT}$ sample was refluxed in 50 mL of concentrated HCl (37%, Aldrich) at 100ºC for 24 h. Then sample was filtered, gently washed with deionized water and dried at 60 ºC for 24 h.

2.2. Characterization of Materials

The structural characterization of materials was performed by powdered X-ray diffraction (XRD) in a Philips X'Pert diffractometer (Eindhoven, The Netherlands) equipped with CuK_α (40 kV, 20 mA) over the range from 0.6 to 6.0º with a step of 0.02º and a contact time of 5 s. Electron microscopy was carried out in a JEOL 3000FEG transmission electron microscope operating at 300 kV and fitted with a X-ray energy dispersive spectrometer (EDS) (Oxford Instruments).

The textural properties of materials were determined by N_2 adsorption porosimetry. The N_2 adsoption/desorption analyses were carried out at -196 ºC on a Micromeritics ASAP2020 analyzer (Micromeritics Co., Norcross, USA). In all cases, 50-70 mg of material was degasses at 80 ºC for 24 h under a vacuum lower than 0.3 kPa before the analysis. The surface area (S_{BET}) was determined from adsorption data obtained at P/P_0 between 0.05 and 0.2 by using the Brunauer-Emmett-Teller (BET) method.[30] The total pore volume was estimated from the amount of N_2 adsorbed at a relative pressure of 0.97, assuming that adsorption on the external surface was negligible compared to adsorption in pores. To assess the possible existence of micropores (pore diameter < 2 nm) in samples, the *t*-plot method was employed,[31] which allowed the estimation of the microporous fraction contributions, $V_{\mu P}$ and $S_{\mu P}$, to the total pore volume and surface area, respectively. The average mesopore size (D_P) was obtained from the maximum of the pore size distribution calculated from the adsorption branch of the isotherm using the BJH method.[32] The wall thickness (t_{wall}) was calculated by using the expression $t_{wall} = a_0 - D_P$, where a_0 is the unit cell parameter calculated from the d_{10} value of XRD using the expression $a_0 = d_{10} \times 2/\sqrt{3}$.[33]

The existence of functional groups and their chemical nature were investigated by Fourier transform infrared spectroscopy (FTIR) in a Thermo Nicolet Nexus spectrometer equipped with a Goldengate attenuated total reflectance (ATR) device (Thermo scientific, USA). Quantitative determination of phosphorus in functionalized samples was determined by using X-ray fluorescence spectroscopy (XRF) in a Philips PANanalytical AXIOS spectrometer (Philips Electronics NV). X-ray were generated using the R_hK_α line at $\lambda = 0.614$ Å. The amount of residual surfactant in samples was calculated from elemental chemical analysis and thermal analyses (TG and DTA). Elemental chemical analysis was carried out in a Perkin-Elmer 2400CHNS thermo

analyzer (Perkin-Elmer, USA). Thermal analyses were conducted under a dynamic air atmosphere between 30 and 950 ºC (flow rate 50 mL min^{-1} with a heating rate of 10 ºC min^{-1}) using a Perkin Elmer Diamond analyzer (Perkin-Elmer, USA).

To investigate the cross-linking degree and the amount of silanol groups present in the synthesized materials ^{29}Si magic angle spinning (MAS) solid-state nuclear magnetic resonance (NMR) measurements were performed in a Bruker AV-400-WB spectrometer (Karlsruhe, Germany) operating at 79.49 MHz. Solid samples were placed in a 4 mm zirconia rotor and spun at 10 kHz. Chemical shifts (δ) of ^{29}Si were externally referred to 3-trimethylsilyl-1-propanesulfonic acid sodium salt (DDS) at δ = 0.0 ppm. Time periods between successive accumulations were 5 ms and *ca.* 15 000 scans were collected. The population of silanol groups per mole of silica was calculated from the relative population of silanol and germinal species, and divided by the weight per mol of silica materials (Eq. 1).[34] The weight is derived from the relative populations and effective molecular weights (EMW) of the silanol, germinal, and siloxane species. The effective molecular weight of each species (EMW_Q) is defined as the sum of the molecular weight of the atoms contributing to each species with the oxygen atoms in the siloxane bridges (Si–O–Si) that connect the species counted by half. The equation is:

$$[SiOH] = \frac{(2\times\%Q^2) + \%Q^3}{(\%Q^i \times \mathrm{EM}W_Q)} \qquad \text{(Eq. 1)}$$

Where [SiOH] is the silanol group concentration in mol g^{-1} and $\%Q^i$ is the relative population of species Q^i (Q^2, Q^3 and Q^4).

$^1H \rightarrow ^{13}C$ and $^1H \rightarrow ^{31}P$ CP (cross-polarization)/MAS solid state NMR measurements were performed to evaluate the different carbon and phosphorus environments, respectively, in the synthesized samples. Samples were spun at 12 kHz for ^{13}C and 6 kHz for the case of ^{31}P. The spectrometer frequencies were set to 75.45 and 161.97

MHz for ^{13}C and ^{31}P, respectively. Chemical shift values were referenced to glycine and phosphoric acid (H_3PO_4) for ^{13}C and ^{31}P, respectively. All spectra were obtained by proton enhanced CP employing a contact time of 1 ms. The time period between successive accumulations was 3 s and 4 s for ^{13}C and ^{31}P, respectively, and the number of scans was *ca.* 15 000 for all spectra.

To investigate the surface charge properties of materials in aqueous media, zeta-potential (ζ)-measurements at different pH values were performed on a Malvern Zetasizer Nano Series instrument (UK). For this purpose, 5 mg of each powdered sample was added to 5 mL of KCl 10 mM (used as the supporting electrolyte) and the pH was adjusted by adding appropriate volumes of 0.10 M HCl or 0.10 M KOH solutions.

2.3. *In vitro* Drug Loading and Release

Cephalexin (CPX) was chosen as model drug for loading and release assays. CPX loading assays were carried out by soaking 250 mg of powder samples in 10 mL of a 20 mM CPX solution in water (pH = 6) for 40 hours under magnetic stirring. Then samples were filtered, gently washed with deionized water and dried at room temperature under vacuum for further 24 hours. The presence of CPX in powdered samples was assessed by FTIR spectroscopy and the amount of drug loaded was determined by CHNS elemental chemical analysis.

To carry out in vitro CPX release assays, 35 mg of each drug loaded powder sample was compacted into disks of 6 mm in diameter and 2 mm in height by using uniaxial pressure at 2.75 MPa. Then, the disks were hung in screw caps using platinum wire and soaked into tubes containing 2 mL of phosphate buffer saline (PBS, Sigma-Aldrich, pH

7.4). The solution was kept at 37 ºC and, to avoid limitations of the delivery rate by external diffusion constraints, continuous orbital stirring at 150 rpm was maintained during the assays. After certain intervals of time, samples were removed from PBS and placed in tubes containing 2 mL of fresh PBS. The cumulative CPX released was determined by UV-Vis spectroscopy by measuring the absorbance signal at 251 nm in a Unicam UV500 spectrometer (Gemini BV, Germany). CPX solutions in PBS with concentrations in the 0.01–0.2 mg mL^{-1} range were used for calibration. The curve was linear with a relationship of absorbance = 13.95 [CPX] (correlation coefficient = 0.998). The apparent drug release was normalized to the amount of drug loaded within the samples to calculate the relative amount of drug release. The CPX concentration was determined from the average of the readings from three different samples (N = 3), and data were presented as mean ± standard deviation.

3. Results and Discussion

3.1. Materials Characterization

The chemical nature of samples was investigated by using FTIR, CHNS elemental chemical analysis, XRF and solid-state NMR spectroscopy. Fig.1.A displays FTIR spectra of samples before ($SBA15_{DPT}$) and after (HCl-$SBA15_{DPT}$) being submitted to the HCl treatment. All spectra show a broad band at around 3400 cm^{-1} corresponding to the overlapping of the O–H stretching bands of hydrogen-bonded water molecules (H–O–H) and SiO–H stretching of surface silanols hydrogen bonded to molecular water (SiO–H ••• OH_2). The O–H bending vibration mode of these adsorbed water molecules account for the band centered at 1630 cm^{-1}. In addition, the Si–O in-plane stretching vibrations of the silanol Si–OH groups appear at 960 cm^{-1}, whose reasonably high intensity points to the relatively low polymerization degree of the silica matrices. The

relative intensity of this band is slightly smaller in HCl-SBA15$_{DPT}$ than in SBA15$_{DPT}$, which would account to a higher condensation degree of the silica matrix in the former, in agreement with ^{29}Si MAS solid state NMR studies (vide infra). The intense silicon-oxygen covalent bond vibrations appearing in the 1100-1000 cm^{-1} range confirm the existence of a silica network, where oxygen atoms play the role of bridges between two silicon atoms. Besides, the symmetric stretching vibration of Si–O–Si and its bending mode appear at *ca.* 800 and 440 cm^{-1}, respectively.[35] The band at 560 cm^{-1} is assigned to Si–O stretching of the silica network defects.

The incorporation of ethylphosphonate groups (–$(CH_2)_2PO(OCH_2CH_3)_2$) into SBA15$_{DPT}$ sample and their transformation to ethylphosphonic acid moieties (–$(CH_2)_2PO(OH)_2$) after acid treatment in HCl-SBA$_{DPT}$ sample can be confirmed by FTIR spectroscopy. The ≡Si–$(CH_2)_2PO(OCH_2CH_3)_2$ fragments in SBA15$_{DPT}$ sample are reflected in the FTIR spectra as the group of three bands with moderate intensities within the 3000-2800 cm^{-1} and weakly intense bands within the 1490-1350 cm^{-1} range (see Fig.1.B for a magnification of the FTIR spectrum in the 1600-1300 cm^{-1} region). The former are characteristic of asymmetric and symmetric C–H stretching vibrations, whereas the absorption bands at 1480 cm^{-1}, 1450 cm^{-1}, 1395 cm^{-1} and 1372 cm^{-1} can be respectively assigned to $\delta(CH_2)$, $\delta_{as}(CH_3)$, $\delta_s(CH_3)$ and $\omega(CH_2)$ vibrations of ethoxy groups bounded to phosphorus. The band with moderate intensity at 1414 cm^{-1} is characteristic of CH_2 vibrations related to Si-CH_2 fragments.[36] The ν(P=O) absorption band appears as a shoulder at 1215 cm^{-1}. The low-frequency shift compared to pure DPT (*ca.* 1241 cm^{-1}) suggests the participation of phosphoryl groups in the formation of hydrogen bond.

The successful conversion of –$PO(OCH_2CH_3)_2$ into –$PO(OH)_2$ groups after treatment of SBA15$_{DPT}$ sample with HCl is evidenced in the FTIR spectrum of HCl-SBA15$_{DPT}$, which exhibit distinct differences from that of SBA15$_{DPT}$ (Fig.1). First, the three peaks

at 3000-2800 cm^{-1}attributed to C-H vibrations become very weak. In addition, the bands in the 1490-1350 cm^{-1} region related to vibration modes of ethoxy groups bonded to phosphorus site of DPT almost completely disappear. Only the band at 1414 cm^{-1} related to $–Si(CH_2)_2–P–$ fragments is clearly observed.

XRF analyses provided the phosphorus content in samples, which allowed determining the number of functional groups present in samples, being 1.5 and 2.5 the density of $≡Si–(CH_2)_2PO(OCH_2CH_3)_2$ and $≡Si–(CH_2)_2PO(OH)_2$ groups per nm^2 for $SBA15_{DPT}$ and HCl-$SBA15_{DPT}$ samples, respectively (Table 1). These findings are in good agreement with the nominal values of 1.7 and 2.3 functional groups per nm^2 for $SBA15_{DPT}$ and HCl-$SBA15_{DPT}$ samples, respectively, which have been calculated on the basis of the 0.85/0.15 TEOS/DPT nominal molar ratio used during the synthesis and taking into account the experimental surface areas ($S_{BET,}$ Table 1). CHNS elemental analyses allowed determining the amount of residual surfactant in samples, being 4.2% and 0.3% in $SBA15_{DPT}$ and HCl-$SBA15_{DPT}$, respectively, which accounts for the almost complete template removal in the latter aided by the acid treatment.

The nature and status of phosphonate groups in samples was also investigated by solid state NMR spectroscopy. $^{1}H \rightarrow {}^{13}C$ CP-MAS solid state NMR was used to confirm the presence of organic functional moieties and the removal of surfactant from samples. In this work it is also a valuable tool to determine if the ethoxy groups on the phosphorus sites of DPT are hydrolyzed after the HCl treatment and therefore phosphonate groups from DPT in $SBA15_{DPT}$ are converted to phosphonic acid groups in HCl-$SBA15_{DPT}$. As expected, signals attributed to the residual surfactant are found in the $^{1}H \rightarrow {}^{13}C$ NMR spectrum of $SBA15_{DPT}$ (indicated by asterisks in Fig.2), in agreement with the results derived from elemental chemical analyses. In the $^{1}H \rightarrow {}^{13}C$ CP-MAS NMR spectrum of $SBA15_{DPT}$ two intense resonances at 5.9 and 20.0 ppm represent the ethyl carbon atoms

C1 and C2, which are those linked directly to silicon (–Si–*C*H_2–CH_2–P–) and phosphorus (–Si–CH_2–*C*H_2–P–), respectively.[36,37] The $^{1}H \rightarrow {}^{13}C$ CP-MAS NMR spectrum of $SBA15_{DPT}$ sample displays another two well-defined peaks at 65.0 and 17.8 ppm respectively assigned to α and β carbons of ethoxy groups on the phosphorus site of the phosphonate groups. After treatment with HCl, the almost total disappearance of such resonances in the NMR spectrum confirms that practically all the ethoxy groups have been successfully converted to hydroxyl groups in HCl-$SBA15_{DPT}$ (Fig. 2).

$^{1}H \rightarrow {}^{31}P$ CP-MAS solid state NMR spectra of samples (Fig. 3) display two main peaks centered at around 33 and 22 ppm, which indicate that there are two distinct local environments of the ^{31}P nuclei. The peak appearing at 33.5 ppm in $SBA15_{DPT}$ slightly shifts towards upfield (31.5 ppm) in HCl-$SBA15_{DPT}$ spectrum, which can be attributed to the transformation of phosphonate ($PO(OEt)_2$) to phosphonic acid ($PO(OH)_2$ or PO(OH)(OEt)) groups.[38] The peak appearing at *ca.* 22 ppm in both samples is a consequence of surface interactions between the phosphorus containing groups and the silica framework, *i.e*. formation of hydrogen bond with the silanol groups (Si–OH) present in the silica matrix.[37] The intensity ratios for the *ca.* 32 peak to the 22 ppm peak are 93:7 and 73:27 for $SBA15_{DPT}$ and HCl-$SBA15_{DPT}$, respectively, suggesting and increase in the number of phosphonic acid groups that are engaged in hydrogen bonding after treatment with HCl.

To evaluate the chemical grafting of organosiloxane to the silica network and the silica condensation degree, ^{29}Si MAS-NMR spectroscopy measurements were carried out. Tetra-functional silicon centers were named with the conventional Q^n notation, where Q refers to $[(SiO)_nSi(OX)_{4-n}]$ units, *n* being the number of bridging oxygen atoms surrounding the central silicon atom and X = H or CH_2CH_3. Likewise, tri-functional silicon centers were named with the conventional T^m notation, where T refers to

$[(SiO)_mRSi(OX)_{3-m}]$ units, *m* being the number of bridging oxygen atoms surrounding the central silicon atom, X = H or CH_2CH_3 and R = $–(CH_2)_2–PO(OCH_2CH_3)_2$ or $≡Si–(CH_2)_2–PO(OH)_2$. The relative populations of silicon environments were calculated by deconvolution of the ^{29}Si NMR spectra into individual Gaussian peaks. The assignation of the resonance signals from the spectra is displayed Fig. 3 and the relative peak areas are shown in Table 2. All spectra display five signals at *ca.* -94, -103 and -113 ppm, corresponding to Q^2, Q^3 and Q^4 species, and at *ca.* -62 and -69, corresponding to T^2 and T^3 sites, at the relative intensities displayed in Table 2. The presence of these two latter signals confirms the existence of covalent bonds between the silica surface and the organic groups. From the normalized peak areas, the relative abundance of T^m species the molar functionalization degree, $\%F = T^m/(T^m+Q^n)$, can be calculated, being 15% and 12% for $SBA15_{DPT}$ and HCl-$SBA15_{DPT}$ samples, respectively, in close agreement with the nominal one based on the composition of the initial mixture (15%). For HCl-$SBA15_{DPT}$ higher Q^4/Q^3 values are obtained (Table 2), which is associated to a significant decrease in the intensity of Q^3 and Q^2 species. Actually, there is a 16% increase in the relative intensity of Q^4 species in HCl-$SBA15_{DPT}$ sample compared to $SBA15_{DPT}$ material, in agreement with the decrease with the number of silanol groups and therefore and increase in the silica condensation degree of the former. These findings agree with the results derived from FTIR, where the relative intensity of the vibration bands ascribed to silanol groups decreased in the spectra of acid-treated sample. Previous reports have demonstrated that two pathways could contribute to the increase in the intensity of the Q^4 species after treatment with HCl.[38] One is the formation of cyclic P–O–Si (Q^4) resulting from the side reaction of PO_3H_2 groups and neighboring Q^2 and/or Q^3 groups, and the other is the further condensation of Q^2 and Q^3 silanols.

Once investigated the chemical nature of samples, their structural characterization was carried out. XRD patterns at small angles of $SBA15_{DPT}$ and HCl-$SBA15_{DPT}$ samples display well resolved peaks at $1:3^{1/2}:2$ d-spacing ratios (Fig. 4), which can be indexed as 120, 110 and 210 reflections, respectively of a well-ordered 2D-hexagonal structure with *p6mm* plain groups typical of SBA-15. The increase of *d*(100) spacing in HCl-$SBA15_{DPT}$ compared to that in $SBA15_{DPT}$ indicates the lattice expansion of the material after being submitted to the HCl reflux. This phenomenon has been previously reported for other mesoporous organosilicas functionalized with phosphonate moieties and treated with concentrated HCl.[39]

Fig.5.A displays the N_2 adsorption-desorption isotherms of samples. Both of them can be identified as type IV isotherms, according to the IUPAC classification, with clear H1-type hysteresis loops at relative high pressure that indicate the existence of open-ended cylindrical mesopores with narrow pore size distributions, which are characteristic of SBA-15 type materials.[31,33] The main textural features derived from the appropriate treatment of N_2 adsorption data are summarized in Table 1. It should be noticed that the surface area (S_{BET}) of HCl-$SBA15_{DPT}$ sample (364 m^2/g) experiences a decrease of 25% with respect to that of $SBA15_{DPT}$ (466 m^2/g). The total pore volume (V_P) is preserved, being *ca.* 5 cm^3/g for both samples, although there is a decrease in the micropore volume in HCl-$SBA15_{DPT}$. The pore diameters (D_P) are 7.4 and 8.7 nm for $SBA15_{DPT}$ and HCl-$SBA15_{DPT}$, which points to and enlargement of the mesopore size and a broadening in the pore size distribution of the material after the acid treatment (Fig. 5.B). Nonetheless, as the network lattice (a_0) also experiences an expansion after the HCl reflux, the wall thickness (t_{wall}) remains constant, *ca.* 5 nm, for both materials.

XRD and N_2 adsorption porosimetry studies indicate that even after being submitted to the relative harsh acidic conditions, HCl-$SBA15_{DPT}$ sample preserves the well-

ordered 2D hexagonal structure typical of SBA-15, whereas only exhibits slight modifications in its textural properties compared to $SBA15_{DPT}$. Accordingly, HCl-$SBA15_{DPT}$ shows slightly smaller surface area (S_{BET}), micropore area ($S_{\mu P}$) and micropore volume ($V_{\mu P}$), and greater pore diameter than $SBA15_{DPT}$ sample.

3.2. *In vitro* drug loading and release

To investigate the performance of both matrices as drug delivery devices, their adsorption and release behavior was *in vitro* evaluated using cephalexin (CPX) as model drug. Loading assays were carried out by soaking powdered samples in water (pH ~ 6), and CPX release experiments were carried out at the physiological pH of 7.4.[40] In the aqueous medium the CPX molecule exhibit different ionization states depending on the pH, which is due to the presence of one carboxylic acid group and one amine group into its structure (Fig. 6).

With the aim of understanding the interaction of CPX with the different mesoporous samples, the possible ionization equilibria in aqueous media and their corresponding constants depending on the grafted functional groups are displayed below:

$$\text{–Si–OH} + H_2O \leftrightarrows \text{–Si–O}^- + H_3O^+ \quad \text{(Eq. 2)}$$

(deprotonation of Q^3 silanol groups pKa ~2-4.5, ref. [41])

$$\text{–Si–OH} + H_2O \leftrightarrows \text{–Si–O}^- + H_3O^+ \quad \text{(Eq. 3)}$$

(deprotonation of Q^2 silanol groups pK_a~8.5, ref. [41])

$$\text{–}PO_3H_2 + H_2O \leftrightarrows \text{–}PO_3H^- + H_3O^+ \quad \text{(Eq. 4)}$$

(1^{st} deprotonation of phosphonic acid groups pKa ~ 2-3; ref. [42])

$$\text{–}PO_3H^- + H_2O \leftrightarrows \text{–}PO_3^{2-} + H_3O^+ \quad \text{(Eq. 5)}$$

(2^{nd} deprotonation of phosphonic acid groups pKa ~ 7-8; ref. [42])

To get information about the net surface of mesoporous materials, ζ-potential measurements were recorded at different pH values, being *ca.* -32 mV and *ca.* -36 mV the values respectively found at pH of 6 and 7.4 for both samples. The similar ζ-potential found values can be explained by the almost equal number of ionizable –OH groups present in both materials, which provide the surface of samples of Brönsted acid character (Table 1). $SBA15_{DPT}$ sample exhibit 10.6 -SiOH per nm^2. On the other hand, HCl-$SBA15_{DPT}$ possesses lower number of –SiOH (9.0 per nm^2) but it also exhibits 2.5 ionizable $–PO_3H_2$ groups per nm^2. These organic groups are responsible of the net negative charge present in the materials both at the loading and the release pH.

The amount of CPX loaded into mesoporous samples was quantified by elemental chemical analyses, being 21.9 and 39.0 mg/g for $SBA15_{DPT}$ and HCl-$SBA15_{DPT}$ samples, respectively (Table 3). As previously mentioned, the main forces that govern the adsorption of molecules on mesoporous silicas are electrostatic or Coulombic interactions, hydrogen bonding and non-polar interactions.[43] In this particular case, non-polar interactions are not the driving forces, because both CPX and the matrices synthesized in this work possess a principally hydrophilic character. At the loading pH of 6, *ca.* 86% of CPX is found as *zwitterionic* specie ($CPX^{\pm}$), where the amino group is protonated as $–NH_3^+$ and the carboxylic acid group is deprotonated as $–COO^-$. Thus, only 14% of CPX molecules would exist as positive charge species. Therefore, different electrostatic attracting interactions and H-bonding take place between CPX and both $SBA15_{DPT}$ and HCl-$SBA15_{DPT}$ materials. The protonated amino group ($–NH_3^+$) from *zwitterionic* $CPX^{\pm}$ is capable of interacting with deprotonated silanol groups (SiO^-) present in the mesoporous walls. Besides, this $–NH_3^+$ group (hydrogen bond donating group) can also interact via hydrogen bonding with phosphoryl group (–P=O) (hydrogen

bond accepting group). Finally, protonated carboxylic groups (–COOH) of CPX^+ can form hydrogen bonds with -SiO^- and P=O groups of mesoporous samples. In the case of HCl-$SBA15_{DPT}$ sample there are additional host-guest interactions that cannot take place in $SBA15_{DPT}$, namely: *i)*electrostatic attracting interactions between $–NH_3^+$ (from $CPX^{\pm}$ and CPX^+) and deprotonated phosphonic acid groups ($–PO^-$); and *ii)* hydrogen bonding between NH_3^+ (from $CPX^{\pm}$ and CPX^+) and phosphonic acid group (–P–OH), between deprotonated carboxylic groups from $CPX^{\pm}$ and –P–OH on materials surface, and carboxylic groups (–COOH) from CPX^+ and $–PO^–$ from mesoporous samples. The extra matrix-drug interactions between CPX and HCl-$SBA15_{DPT}$ compared to those existing in $SBA15_{DPT}$ would account for the greater drug loading in the former, as experimentally found, despite of presenting lower S_{BET}.

In vitro drug release assays were performed in PBS under physiological conditions (pH 7.4 and 37 ºC). Fig. 7 shows CPX release patterns from both mesoporous matrices. The main driving force that usually governs drug departure from mesoporous matrices is pore diffusion/convection, which can be fitted to first order kinetics.[29,44] In addition, the carrier-drug host-guest interactions play a key role in drug release kinetics from mesoporous materials. In this sense, drug molecules may directly interact with mesoporous matrices, lowering their solubility and/or retaining their release. In such a case, drug molecules are termed as associated, which need to be disassociated from nanocarriers prior to release. The association and dissociation processes are assumed to be reversible and also follow first order kinetics. Therefore, the theoretical model adopted in this work considers both first-order diffusion/convection and drug association/dissociation processes.[44] Then, the drug release mechanism can be described by the following equation:

$$\frac{M_t}{M_0} = \frac{k_{off}}{k_{on}+k_{off}}\left(1 - e^{-k_s t}\right) + \frac{k_{on}}{k_{on}+k_{off}}\left(1 - e^{-k_{off} t}\right) \qquad \text{(Eq. 6)}$$

where M_t is the cumulative drug release at time *t*; M_0 is the initial amount of drug; k_s is the rate constant of diffusion/convection; and k_{on} and k_{off} are the rate constants of association and disassociation, respectively. The free energy difference between the free and bound states, ΔG, determines the amounts of initially free and bound drug, and can be calculated by the equation:

$$\Delta G = k_B T ln\left(\frac{k_{on}}{k_{off}}\right) \qquad \text{(Eq. 7)}$$

where, k_B is the Boltzmann's constant and T is the absolute temperature (assumed to be 310 K). In this study, therefore, three parameters, ΔG (instead of k_{on}), k_s and k_{off} were used to describe the cumulative drug release from mesoporous silica materials.

CPX release from $SBA15_{DPT}$ is characterized by a high initial burst release (> 30%) followed by a steady-state release, which corresponds to category III of drug release profiles classification reported by Ye *et al.*[45] The fit of the experimental CPX release patterns from $SBA15_{DPT}$ to Eq. 5 allows determining the experimental values for k_s, k_{on} and k_{off}. Then ΔG was calculated using Eq. 7. The obtained results, which properly fit to the theoretical model (R^2= 0.9995), are summarized in Table 3. The conditions $k_s >> k_{off}$ and $k_s >> k_{on}$ are fulfilled, which indicates that diffusion and convection are not neglected during the steady-state release.

At the physiological pH of 7.4, mainly repulsive host-guest interactions take place between $SBA15_{DPT}$ and CPX. Actually, at such pH, 80% CPX exist in its anionic species (CPX^-), whereas only 20% is present as the *zwitterionic* molecule ($CPX^{\pm}$). The surface of mesoporous material is negatively charged (ζ-potential = -36 mV), which lead to repulsive electrostatic interactions between deprotonated silanol groups ($–SiO^-$) in $SBA15_{DPT}$ and CPX^- bearing $–COO^-$ groups. This leads to a relative high initial burst release, where *ca.* 50% of drug is released during the first 10 hours of assay, which

accounts for the weak CPX-mesoporous matrix association and is in agreement with the positive ΔG value of 0.3×10^{-21}J. This burst release may occur to equilibrate the concentrations in both the release medium and the matrix, albeit it has been also ascribed to the release of the molecules adsorbed in the outer surface of mesoporous matrices [19,20]. k_s provides information about the rate of diffusion/convection, but not about the magnitude of the initial burst release. The model reveals a k_s value of 0.98 h^{-1} for $SBA15_{DPT}$, which accounts for a moderated diffusivity of the drug confined into the mesoporous channels. The carrier-drug host-guest interactions can be related to the k_{off} value, which is 5.7×10^{-23} h^{-1}. The k_{off} value gives information about the steady release following initial burst release, but has no effect on the magnitude of initial burst release. Once the CPX concentration inside mesopores decreases obeying a burst effect, a sustained steady-state release where 93% of CPX is released after 2 weeks of assay occurs.

In principle, CPX release profile from HCl-$SBA15_{DPT}$ mesoporous material would be expected to be similar to that of $SBA15_{DPT}$. This would be supported by the fact that the number of Brönsted acid groups susceptible of undergoing deprotonation is similar, *ca.* 5×10^{-21} groups per gram of material, in both cases (Table 1), being 4.9×10^{-21} –SiOH per gram of material for $SBA15_{DPT}$ and 3.3×10^{-21} –SiOH and 1.8×10^{-21} –POH per gram for HCl-$SBA15_{DPT}$. This also agrees with the ζ-potential values determined for both samples at pH 7.4 of *ca.* -36 mV, which would account for repulsive electrostatic host-guest matrix-CPX interactions for both samples. On the other hand, XRD patterns of both materials pointed to a well-ordered 2D-hexagonal *p6mm* structure typical of SBA-15. Moreover, the results derived from the treatment of N_2 adsorption data only evidenced slight variations in the textural properties of both materials (Table 1). The slightly greater pore diameter of HCl-$SBA15_{DPT}$ (8.7 nm) compared to that of

$SBA15_{DPT}$ (7.4 nm) could account for a relative higher drug diffusivity of the former. In addition, the relative higher microporosity of $SBA15_{DPT}$ ($S_{\mu P}$ = 35 m^2/g) compared to that of HCl-$SBA15_{DPT}$ ($S_{\mu P}$ = 18 m^2/g) could also contribute to a slower drug release out of the pores in the former. In this sense, drug molecules would be expected to have stronger interactions with the host in the sequestered volume provided by the micropores, which would lead to more sustained release kinetics.[46]

Even though taking into consideration the above-mentioned aspects, drug release profile of HCl-$SBA15_{DPT}$ drastically differs from than that of $SBA15_{DPT}$ (Fig. 7). The curve consists of an abrupt burst release where 100% of the drug is released only after 10 hours of assay. It can be classified as the Case 1 release model reported by Zeng *et al.*,[44] which corresponds to the fast disassociation of drug molecules from the carrier such that $k_{off}>>k_{on}$. As a result, most of the drug molecules are initially free and the drug release profile is determined by diffusion and convection only. In this case, the solution in Eq. 6 can be reduced to:

$$\frac{M_t}{M_0} = 1 - e^{-k_s t} \qquad \text{(Eq.8)}$$

The good fit of the experimental data of drug release from HCl-$SBA15_{DPT}$ to Eq. 8 (R^2 = 0.9991) provides a k_s value of 1.10 h^{-1}, which is only slightly higher than that of SBA_{DPT} (0.98 h^{-1}). This could be explained by the greater pore diameter of the former. Nonetheless, the lack of steady-state release since almost 100% of CPX is released during a burst effect cannot be explained neither considering the chemical nature nor the structural and textural properties of HCl-$SBA15_{DPT}$ derived from XRD and N_2 adsorption studies.

In the search for new insights about possible mesostructural damages that allow explaining the different drug release performance of mesoporous matrices, an

exhaustive study by HRTEM was carried out. In fact, it is difficult to determine alterations in the crystal structures solely from powder XRD data.[47] TEM images and their corresponding FT (Fast Fourier Transform) for $SBA15_{DPT}$ and $HCl\text{-}SBA15_{DPT}$ samples are displayed in Fig. 8 and Fig. 9, respectively. EDS analysis was performed during the TEM observation. Si, O and P peaks appear in both samples. The average P percentage is 3.6 and 1.7 for $SBA15_{DPT}$ and $HCl\text{-}SBA15_{DPT}$, respectively. Fig. 8 confirms that $SBA15_{DPT}$ sample exhibits a honeycomb mesoporous arrangement typical of SBA-15, in agreement with XRD patterns. However, TEM images of $HCl\text{-}SBA15_{DPT}$ reveal that there is a noticeable of loss of the mesostructural order (Fig. 9), with only small crystalline domains. This mesostructure loss in $HCl\text{-}SBA15_{DPT}$ due to the acid treatment, which was not detected by XRD, would explain the very different drug release profile of this sample. Albeit the extent of mesostructural order does not affect drug loading, since as above mentioned acid-treated sample loads higher amounts of CPX than untreated sample, it plays a pivotal role in drug release kinetics from mesoporous matrices.

Nonetheless there is another factor that should be also taken into account, since it has been reported that mesoporous matrices can undergo degradation when soaked in diverse fluids under physiological conditions.[48,49,50] A previous study carried out by our research group[49] aimed at comparing the degradation of several SBA-15 type mesoporous materials, *i.e.* pure silica SBA-15 and SBA-15 functionalized with alkoxysilanes bearing different organic groups such as aminopropyl, methyl or octyl. The results indicated that whereas SBA-15 was partially soluble in all tested media, organic modification leaded to the decrease in the degradation rate of mesoporous matrices, which was accompanied by preservation of the mesostructural order even after 60 days of assay. It was concluded that this would be an added value when long-term

applications, including drug delivery, are aimed, which require mesoporous matrices with stable mesostructural order. However, the influence of mesoporous matrix degradation on drug release performance was not evaluated, and it is an interesting topic that will be the object of our future investigations.

Herein, with the aim of supporting the fact that host-guest interactions and mesostructural order are the driving factors that govern CPX release profiles, we have synthetized pure silica SBA-15, SBA-15 functionalized by co-condensation route using an alkoxysilane bearing primary and secondary amine groups (N-(2-aminoethyl)-3-aminopropyl-trimethoxysilane, DAMO) (affording $SBA15_{DAMO}$), and a SBA-15 bifunctionalized by co-condensation using DPT and DAMO (affording $SBA15_{DPT/DAMO}$) (see *supplementary material* for further detail about the synthetic procedure). Portions of these materials were submitted to acidic treatment with 12M HCl under reflux and the resulting samples were respectively denoted as HCl-SBA-15, HCl-$SBA15_{DAMO}$ and HCl-$SBA15_{DPT/DAMO}$. Deep characterization of all materials by elemental chemical analysis, FTIR and NMR indicated the presence of the corresponding functionalities, whereas XRD and N_2 adsorption again pointed to well-ordered SBA-15 mesoporous structures in all cases. Nonetheless, in a similar fashion than occurred with HCl-$SBA15_{DPT}$, HRTEM revealed that the mesostructural order has been notably damaged in HCl-treated materials due to the harsh acidic conditions (Figs. S1, S2 and S3).

All samples, before and after HCl treatment, were loaded with CPX and *in vitro* release tests were performed in PBS (pH 7.4) at 37ºC. Results clearly indicate that the intensity of the host-guest interactions govern drug release profiles from samples non-submitted to acidic treatment. The slower and incomplete release in the tested time was obtained for $SBA15_{DAMO}$ due to the electrostatic attractive interactions between protonated amino groups ($>NH_2^+$ and $-NH_3^+$) and $-COO^-$ of CPX at physiological pH (Fig. S2).

$SBA15_{DPT/DAMO}$ exhibited the second slower release and also incomplete, by the coexistence of attractive (protonated amines of matrix and $–COO^-$ of CPX) and repulsive forces ($–SiO^-$ of the matrix and $–COO^-$ of CPX) (Fig. S3). Lastly a sustained release when the total amount of drug is released after 350 hours of assay is achieved for SBA-15 (Fig. S1), due to the presence of repulsive forces between deprotonated silanol groups of the matrix and $–COO^-$ of CPX. The different CPX delivery profiles for SBA-15 and $SBA15_{DPT}$ could be ascribed to the different extent of degradation of the matrices, being greater in the former. This would be in agreement with the above mentioned published reports. [49]

Finally, CPX release assays for all materials submitted to HCl treatment revealed that all drug release profiles are similar, obeying an initial burst where 100% of the loaded drug is released a few hours of assay for all materials (Figs. S1, S2 and S3).

All these findings demonstrate that the partial loss of mesostructure, which can be only detected by HRTEM, drastically affects drug delivery by promoting the complete drug delivery during a fast burst release effect.

4. Conclusions

Deep characterization of mesoporous materials by HRTEM is indispensable to understand their performance as drug delivery devices. This tool becomes of foremost relevance to study functionalized mesoporous samples that have to be submitted to harsh post-synthesis treatments to attain certain surface organic moieties. This fact has been proved by synthetizing a SBA-15-type mesoporous material functionalized with ethylphosphonate groups and subsequently treating with concentrated HCl to afford ethylphosphonic acid moieties. Although the routine characterization of both materials

by XRD and N_2 adsorption porosimetry points to well-ordered SBA-15 structures, HRTEM studies reveal noticeable mesostructural damage in acid-treated sample. This alteration in the mesopores arrangement is not detected by XRD, probably since this technique gives average information of the full sample. The mesostructural damage dramatically affects drug release profiles from mesopores, giving rise to a fast burst effect where 100% of the loaded molecule is released only after 10 hours of *in vitro* assay. This behavior completely differs from that found in the well-ordered untreated sample which, despite of exhibiting comparable matrix-drug interactions under the release conditions, shows sustained diffusion-controlled drug delivery for more than 2 weeks.

5. Acknowledgements

This study was supported by research grants from Ministerio de Economía y Competitividad (MINECO), Spain, through the projects MAT2012-35556 and CSO2010-11384-E (Agening Network of Excellence). M. Martínez-Carmona also thanks Moncloa Campus of International Excellence (UCM-UPM) for a PICATA predoctoral fellowship. We also thank X-ray Diffraction and Elemental Chemical Analysis C.A.I., UCM.

6. References

[1] M. Vallet-Regí, A. Rámila, R.P. del Real, J. Pérez-Pariente, Chem. Mater. 13 (2001) 308-311.

[2] M. Vallet-Regí, F. Balas, D. Arcos, Angew. Chem. Int. Ed. 46 (2007) 7548-58.

[3] P. Yang, S. Gai, J. Lin, Chem. Soc. Rev. 41 (2012) 3679-3698.

[4] S. Wang, Microporous Mesoporous Mater. 117 (2009) 1-9.

[5] C.G. Trejo, D. Lozano, M. Manzano, J.C. Doadrio, A.J. Salinas, S. Dapía, E. Gómez-Barrena, M. Vallet-Regí, N. García-Honduvilla, J. Buján, P. Esbrit, Biomaterials 31 (2010) 8564-8573.

[6] J. Lu, M. Liong, Z. Li, J.I. Zink, F. Tamanoi, Small 6 (2010) 1794–1805.

[7] F. Tang, L. Li, D. Chen, Adv. Mater. 24 (2012) 1504-1534.

[8] M. Vallet-Regí, M. Colilla, B. González, Chem. Soc. Rev. 40 (2011) 596-607.

[9] H. Yamada, C. Urata, Y. Aoyama, S. Osada, Y. Yamauchi, K. Kuroda, Chem. Mater. 24 (2012) 1462−1471.

[10] T. Asefa, Z. Tao, *Chem. Res. Toxicol. 25* (2012), 2265–2284.

[11] M. Vallet-Regí, M. Manzano, M. Colilla, Biomedical Applications of Mesoporous Ceramics: Drug Delivery, Smart Materials and Bone Tissue Engineering. CRC Press, Taylor & Francis Group, LLC, Boca Raton, 2013.

[1] [12] S. Mura, J. Nicolas, P. Couvreur, Nature Mater. 12 (2013) 991-1003.

[13] A. Baeza, M. Colilla, M. Vallet-Regí, Expert Opin. Drug Deliver. 12 (2015) 319-337.

[14] M. Martínez-Carmona, A. Baeza, M.A. Rodríguez-Milla, J. García-Castro, M. Vallet-Regí, J. Mater. Chem. B. 3 (2015) 5746.

[15] J. Kärgera, R. Valiullin, Chem. Soc. Rev. 42 (2013) 42, 4172-4197.

[16] F. Qu, G. Zhu, S. Huang, S. Li, J. Sun, D. Zhang, S. Qiu, Microporous Mesoporous Mater. 92 (2006) 1-9.

[17] Isabel Izquierdo-Barba, África Martinez, Antonio L Doadrio, Joaquin Pérez-Pariente, María Vallet-Regí, European Journal of Pharmaceutical Sciences, 26 (2005) 365-373.

[18] Jenny Andersson, Jessica Rosenholm, Sami Areva, and Mika Linde´n, *Chem. Mater*. 2004**,** *16*, 4160-4167.

[19] A. Nieto, F. Balas, M. Colilla, M. Manzano, M. Vallet-Regí, Microporous and Mesoporous Materials 116 (2008) 4-13.

[20] F. Balas, M. Manzano, P. Horcajada, M. Vallet-Regí, J. Amer. Chem. Soc. 128 (2006) 8116-8117.

[1] [21] F. Hoffmann, M. Cornelius, J. Morell, M. Fröba, Angew. Chem. Int. Ed. 45 (2006) 3216-3251.

[1] [22] S.-W. Song, K. Hidajat, S. Kawi, Langmuir, 21 (2005) 9568-9575.

[23] A. Nieto, M. Colilla, F. Balas, M. Vallet-Regí, Langmuir 26 (2010) 5038-5049.

[24] S. El Mourabit, M. Guillot, G. Toquer, J. Cambedouzou, F. Goettmann, A. Grandjean, RSC Advances, 2 (2012) 10916-10924.

[25] C.-M Yang, B. Zibrowius, F. Schüth, Chem. Commun. (2003) 1772-1773.

[26] J.M. Rosenholm, M. Lindén, J. Control. Release 128 (2008) 157–164.

[27] R.J.P. Corriu, L. Datas, Y. Guari, A. Mehdi, C. Reyé, C. Thieuleux, Chem. Commun. (2001) 763-764.

[28] D. Zhao, J. Feng, Q. Huo, N. Melosh, G.H. Fredrickson, B.F. Chemelka, G.D. Stucky, Science 279 (1998) 548-552.

[29] M. Colilla, M. Martínez-Carmona, S. Sánchez-Salcedo, L. Ruiz-González, J.M. González-Calbet, M. Vallet-Regí, J. Mater Chem. B 2 (2014) 5639-5651.

[30] S. Brunauer, P.H. Emmett, E. Teller, J. Am. Chem. Soc.60 (1938) 309-319.

[31] S.J. Gregg, K.S.W. Sing, Adsorption, Surface Area, and Porosity, Academic Press, London, New York, 1982.

[32] E.P. Barrett, L.G. Joyner, P.P. Halenda, J. Am. Chem. Soc. 73 (1951) 373-380.

[33] M. Kruk, M. Jaroniec, A. Sayari, Chem. Mater. 11 (1999) 492-500.

[34] B.H. Wouters, T. Chen, M. Dewilde, P.J. Grobet, Microporous Mesoporous Mater. 44-45 (2001) 453–457.

[35] C.J. Brinker, Sol-Gel Science: The Physics and Chemistry of Sol-Gel Processing, Academic Press, Boston, 1990.

[36] O.A. Dudarko, I.V. Mel'nik, Y.L. Zub, A.A. Chuiko, A. Dabrowski, Inorg. Mater. 42 (2006) 360-367.

[1] [37] A. Aliev, D.L. Ou, B. Ormsby, A.C. Sullivan, J. Mater. Chem. 10 (2000) 2758-2764.

[38] Y.-C. Pan, H.-H.G. Tsai, J.-C. Jian, C.-C. Kao; T.-L. Sung, P.-J. Chiuy, D. Saikia, J.-H. Chang, H.-M. Kao, J. Phys. Chem. C. 116 (2012) 1658-1669.

[39] Q. Yang, J. Yang, J. Liu, Y. Li, C. Li, Chem. Mater. 17 (2005) 3019-3024.

[40] M.S. Legnoverde, I. Jiménez-Morales, A. Jiménez-Morales, E. Rodríguez-Castellón, E. I. Basaldella, Med. Chem. 9 (2013), 672-680.

[41] J. M. Rosenholm, T. Czuryszkiewicz, F. Kleitz, J. B. Rosenholm and M. Lindén, Langmuir, 23 (2007) 4315-4323.

[42] A.J. Kresge, Y.C. Tang. J. Org. Chem. 42 (1977) 757-759.

[43] A. Nieto, M. Colilla, F. Balas, M. Vallet-Regí, Langmuir, 26 (2010) 5038-5049.

[44] L. Zeng, L. An, X. Wu. J. Drug Deliver. (2011) Article ID370308, 15 pages.

[45] M. Ye, S. Kim, K. Park, J. Controlled Release, 146 (2010) 241-260.

[46] T. Kjellman, X. Xia, V. Alfredsson, A.E. García-Bennett. J. Mater. Chem. B. 2 (2014) 5265-5271.

[47] O. Terasaki, T. Ohsuna, Z. Liu, Y. Sakamoto, A.E. García-Bennet, Structural study of meso-porous materials by electron microscopy, in: Osamu Terasaki (Ed), Studies in Surface Science and Catalysis, Elsevier, 2004, 148, pp. 261-288.

[48] Q. He, J. Shi, M. Zhu, Y. Chen, F. Chen. Microporous Mesoporous Mater (2010) 314-320.

[49] I. Izquierdo-Barba, M. Colilla, M. Manzano. Microporous Mesoporous Mater., 132 (2010) 442-452.

[50] N. Hao, H. Liu, L. Li, D. Chen, L. Li, F. Tang, J. Nanosci. Nanotechnol. 12 (2012) 6346-6354.

Appendix A. Supplementary material

Supplementary data related to this article can be found at Microporous and Mesoporous Materials website.

Tables

Table 1. Characteristics of the materials synthesized in this work obtained by N_2 adsorption, XRD, XRF and ^{29}Si MAS solid state NMR.

Sample	S_{BET} (m^2/g)	$S_{\mu P}$ (m^2/g)	V_T (cm^3/g)	$V_{\mu P}$ (cm^3/g)	D_P (nm)	a_0 (nm)	t_{wall} (nm)	$^-(CH_2)_2P(O)(OX)_2$ per nm^2	$^-$SiOH per nm^2
$SBA15_{DPT}$	466	35	0.54	0.0093	7.4	12.3	4.9	1.5	10.6
HCl-$SBA15_{DPT}$	364	18	0.55	0.0030	8.7	13.2	4.5	2.5	9.0

S_{BET} and $S_{\mu P}$ are respectively the surface area determined by using the BET method between the relative pressures (P/P_0) 0.05-0.25 and micropore surface obtained using the *t*-plot method. V_P and $V_{\mu P}$ are respectively, the total pore volume and micropore volume obtained using the *t*-plot method. The total pore volume was estimated from the amount of N_2 adsorbed at a relative pressure of 0.97. D_P is the pore diameter calculated by means of the BJH method from the adsorption branch of the isotherm. a_0 is the unit cell parameter calculated by XRD, being $a_0=2/\sqrt{3}.d_{10}$. t_{wall} is the wall thickness calculated using the equation $t_{wall} = a_0 - D_P$. The number of $^-(CH_2)_2P(O)(OX)_2$ groups per nm^2, where X = CH_2CH_3 and X=H for $SBA15_{DPT}$ and HCl-$SBA15_{DPT}$, respectively, was calculated on the basis of XRF. The number of silanol groups (SiOH) was determined by single pulse ^{29}Si solid state NMR spectroscopy, as described in the experimental section.

Table 2. Peak area (%) of T^m and Q^n units from deconvoluting the ^{29}Si MAS NMR spectra $SBA15_{DPT}$ and HCl-$SBA15_{DPT}$ samples. Molar functionalization degree, $\%F = 100\times[T^n/(T^n+Q^m)]$, of samples is also displayed.

	Peak area (%) of Q^n and T^n signals					
Sample	T^2	T^3	Q^2	Q^3	Q^4	$\%F^*$
$SBA15_{DPT}$	5	10	5	35	45	15
HCl-$SBA15_{DPT}$	3	9	3	24	61	12

Table 3. Kinetic release parameters for cephalexin (CPX) release from SBA15DPT and HCl-$SBA15_{DPT}$ materials.

Sample	M_0(mg g^{-1})	k_{off} ($\times10^{-3}$) (h^{-1})	ΔG ($\times10^{-21}$) (J)	k_s (h^{-1})	R^2
$SBA15_{DPT}$	21.9 ± 1.0	5.7 ± 0.2	0.30 ± 0.02	0.98 ± 0.05	0.998
HCl-$SBA15_{DPT}$	39.0 ± 0.4	–	–	1.10 ± 0.03	0.9991

Figure captions

Scheme 1. Schematic description for the synthesis of $SBA15_{DPT}$ and HCl-$SBA15_{DPT}$ samples.

Figure 1. A) FTIR spectra (4000-2500 cm^{-1} and 1800-400 cm^{-1} regions) of $SBA15_{DPT}$ and HCl-$SBA15_{DPT}$ samples. B) Magnification of the FTIR spectra in the 1600-1300 cm^{-1} region.

Figure 2. $^{1}H \rightarrow ^{13}C$ CP/MAS solid state NMR spectra of $SBA15_{DPT}$ and HCl-$SBA15_{DPT}$ samples

Figure 3. ^{29}Si MAS and $^{1}H \rightarrow ^{31}P$ CP/MAS NMR spectra of $SBA15_{DPT}$ and HCl-$SBA15_{DPT}$ samples. The component peaks obtained from spectral deconvolutions are displayed by green dotted lines.

Figure 4. XRD patterns of $SBA15_{DPT}$ and HCl-$SBA15_{DPT}$ samples and indexed reflections for the observed peaks.

Figure 5. A) N_2 adsorption-desorption isotherms and pore size distributions of $SBA15_{DPT}$ and HCl-$SBA15_{DPT}$ samples.

Figure 6. Cephalexin (CPX) species and their relative abundance at the pH values of 6.0 (left) and 7.4 (right), where CPX^{+}, $CPX^{\pm}$ and CPX^{-} represent the cationic, *zwitterionic* and anionic drug species, respectively.

Figure 7. Cephalexin (CPX) release profiles at pH 7.4 (phosphate buffer saline, PBS) for $SBA15_{DPT}$ and HCl-$SBA15_{DPT}$ samples. Error bars represent the standard deviation for three measurements (N = 3)

Figure 8. (A) TEM image; B) EDS spectra; and C) higher magnification TEM image and the corresponding FT (inset) of $SBA15_{DPT}$ sample.

Figure 9. (A) TEM image; B) EDS spectra; and C) higher magnification TEM image and the corresponding FT (inset) of HCl-$SBA15_{DPT}$ sample.

Schemes and Figures

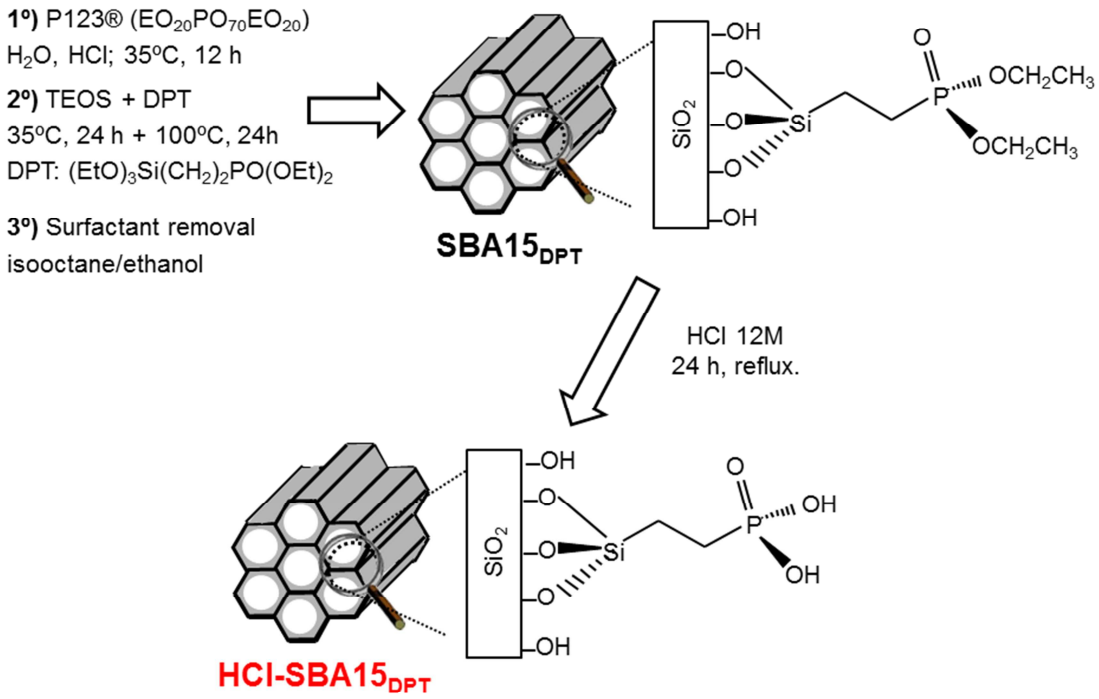

Scheme 1

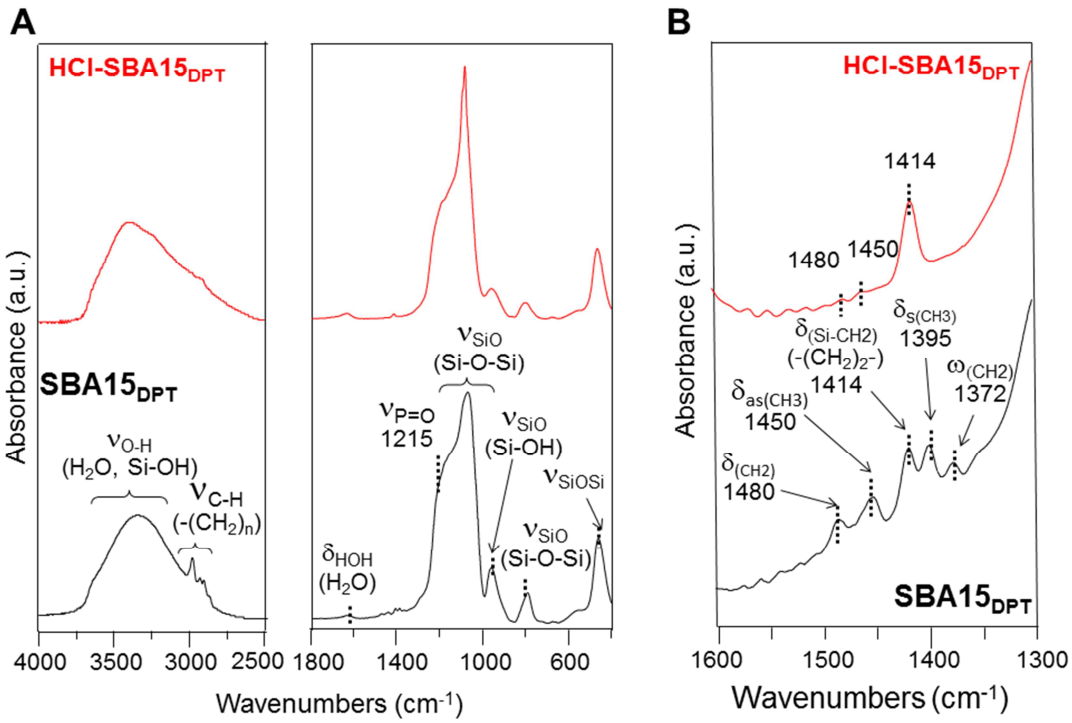

Figure 1

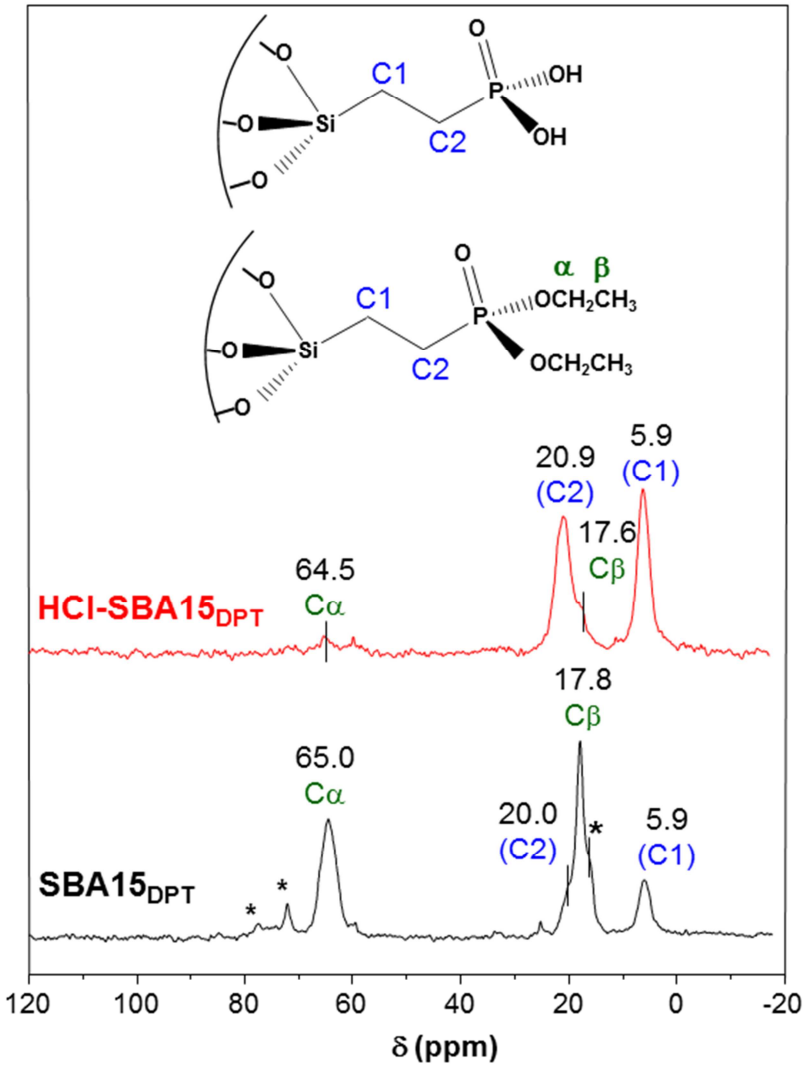
C1
C2
Si
P
OH
OH
O
α β
OCH2CH3
OCH2CH3
20.9
(C2)
5.9
(C1)
17.6
Cβ
64.5
Cα
HCl-SBA15DPT
17.8
Cβ
65.0
Cα
20.0
(C2)
5.9
(C1)
SBA15DPT
*
120
100
80
60
40
20
0
-20
δ (ppm)

Figure 2

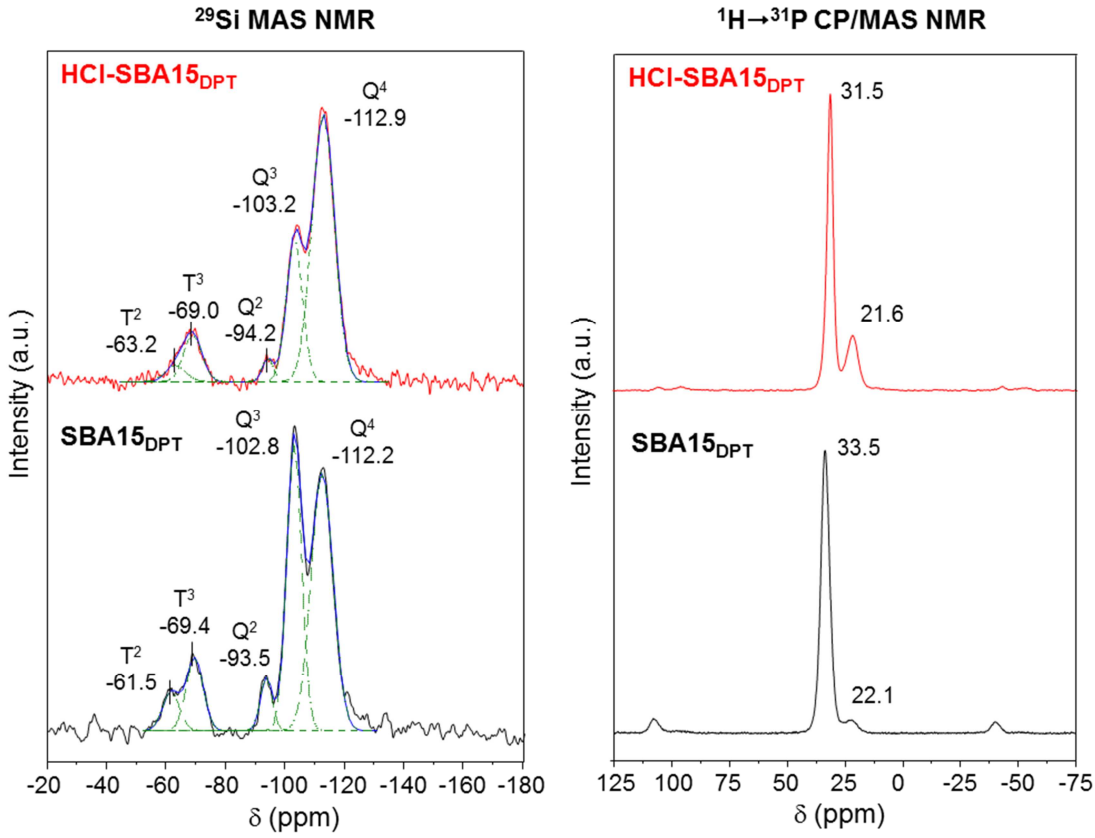

Figure 3

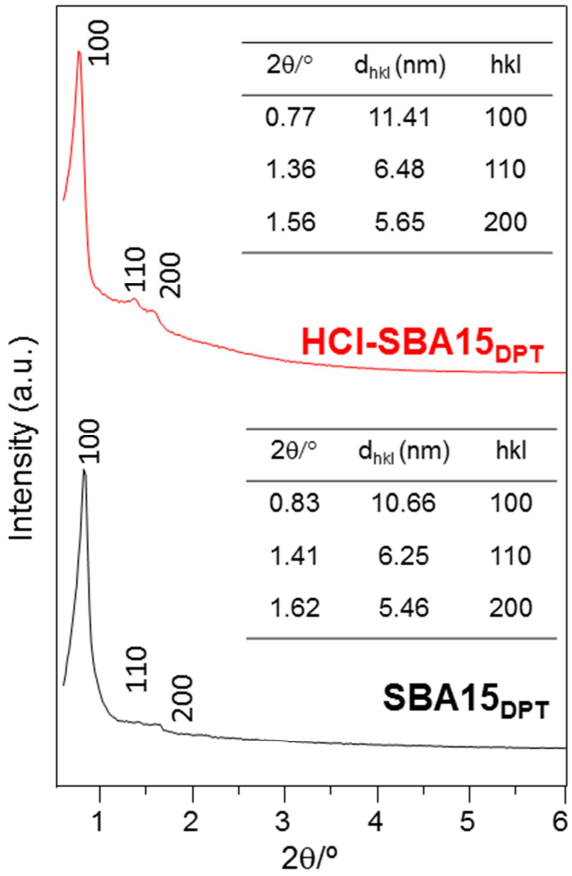

Figure 4

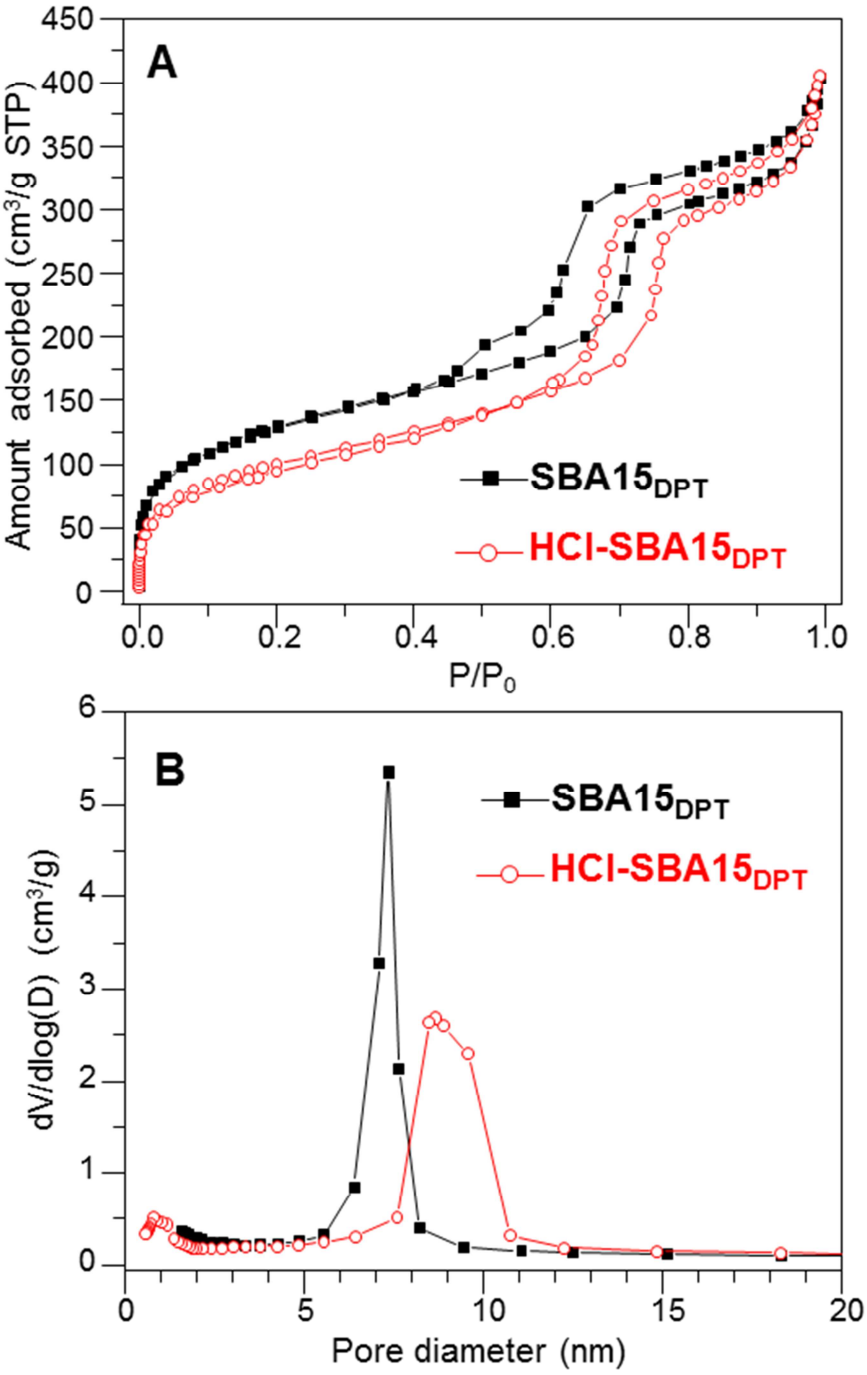
A
Amount adsorbed (cm³/g STP)
P/P0
SBA15DPT
HCl-SBA15DPT
B
dV/dlog(D) (cm³/g)
Pore diameter (nm)
SBA15DPT
HCl-SBA15DPT

Figure 5

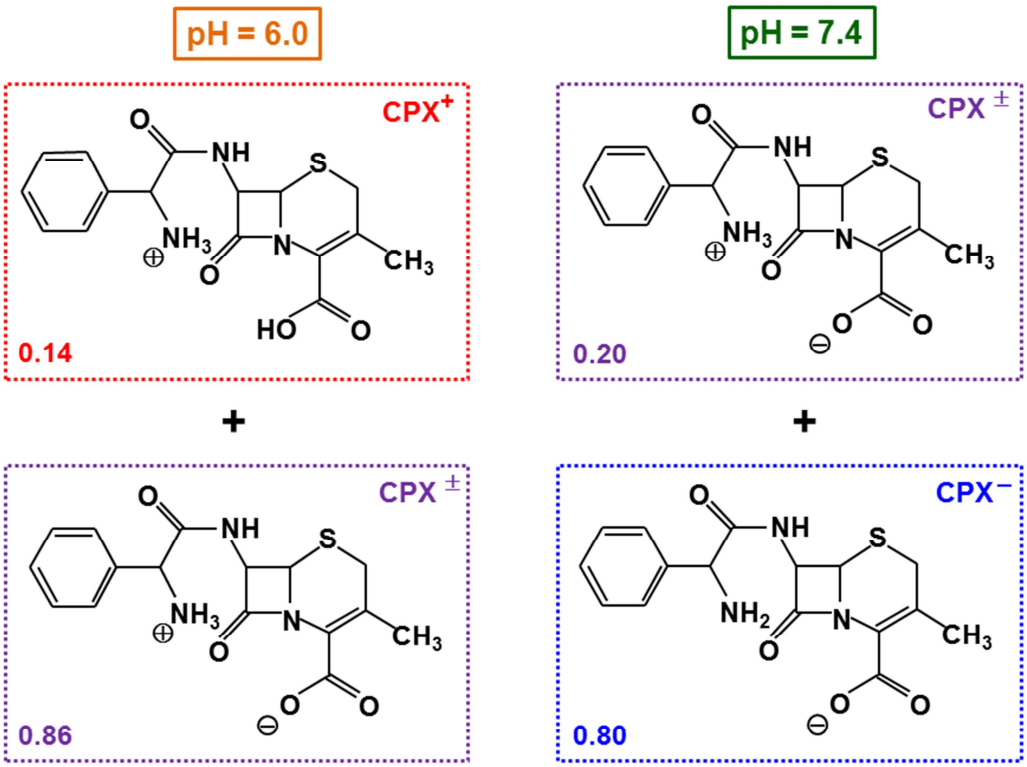

Figure 6

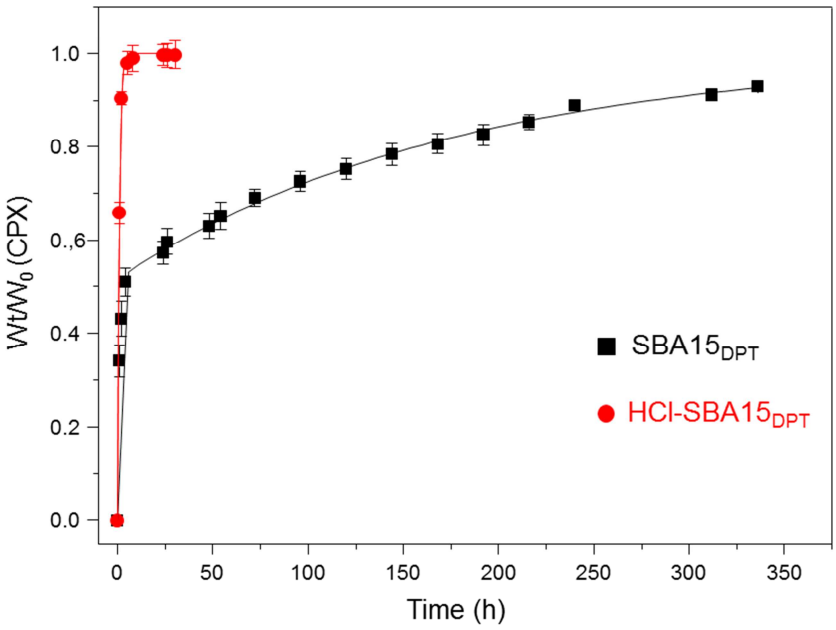

Figure 7

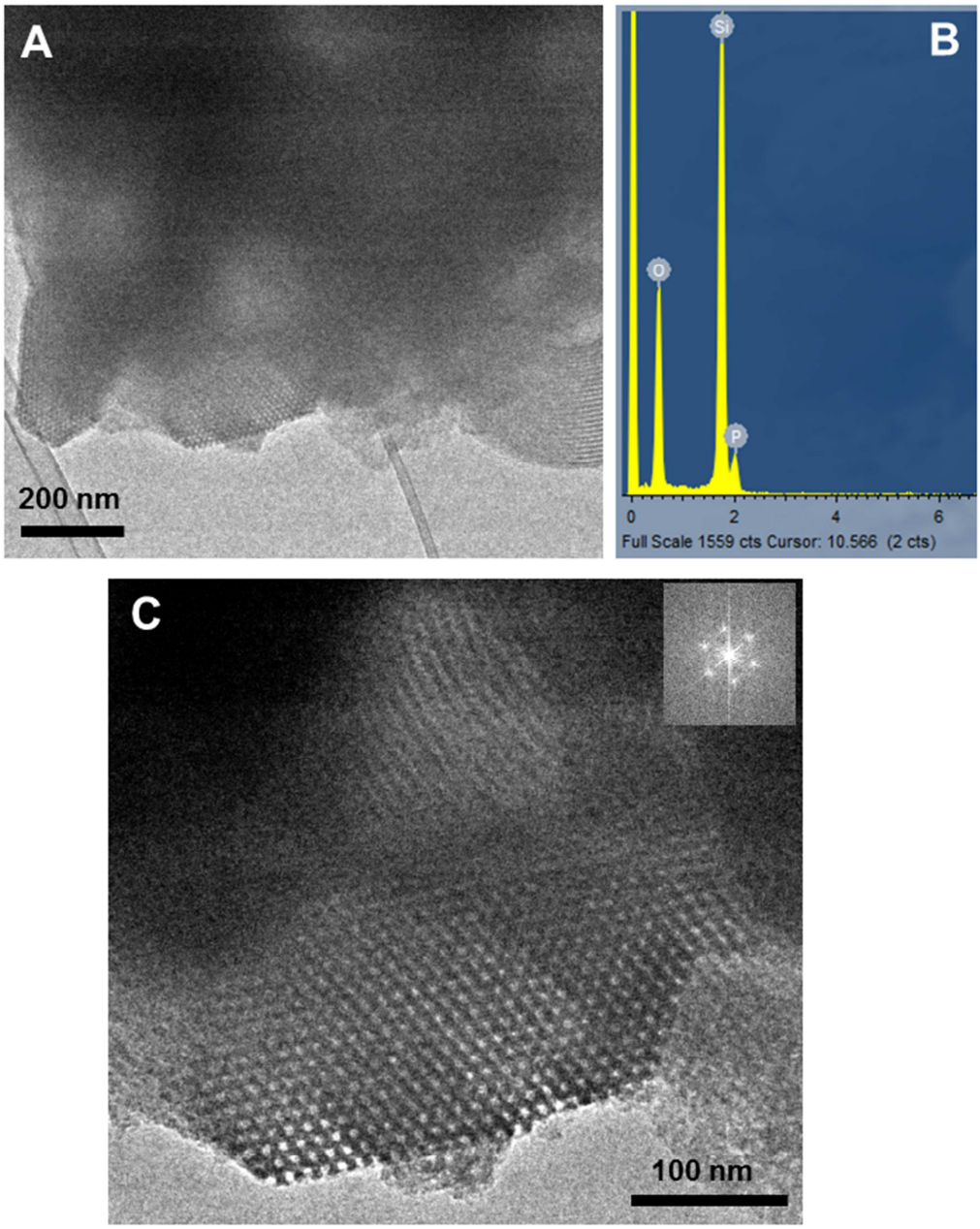
A
200 nm
B
Si
O
P
0
2
4
6
Full Scale 1559 cts Cursor: 10.566 (2 cts)
C
100 nm

Figure 8

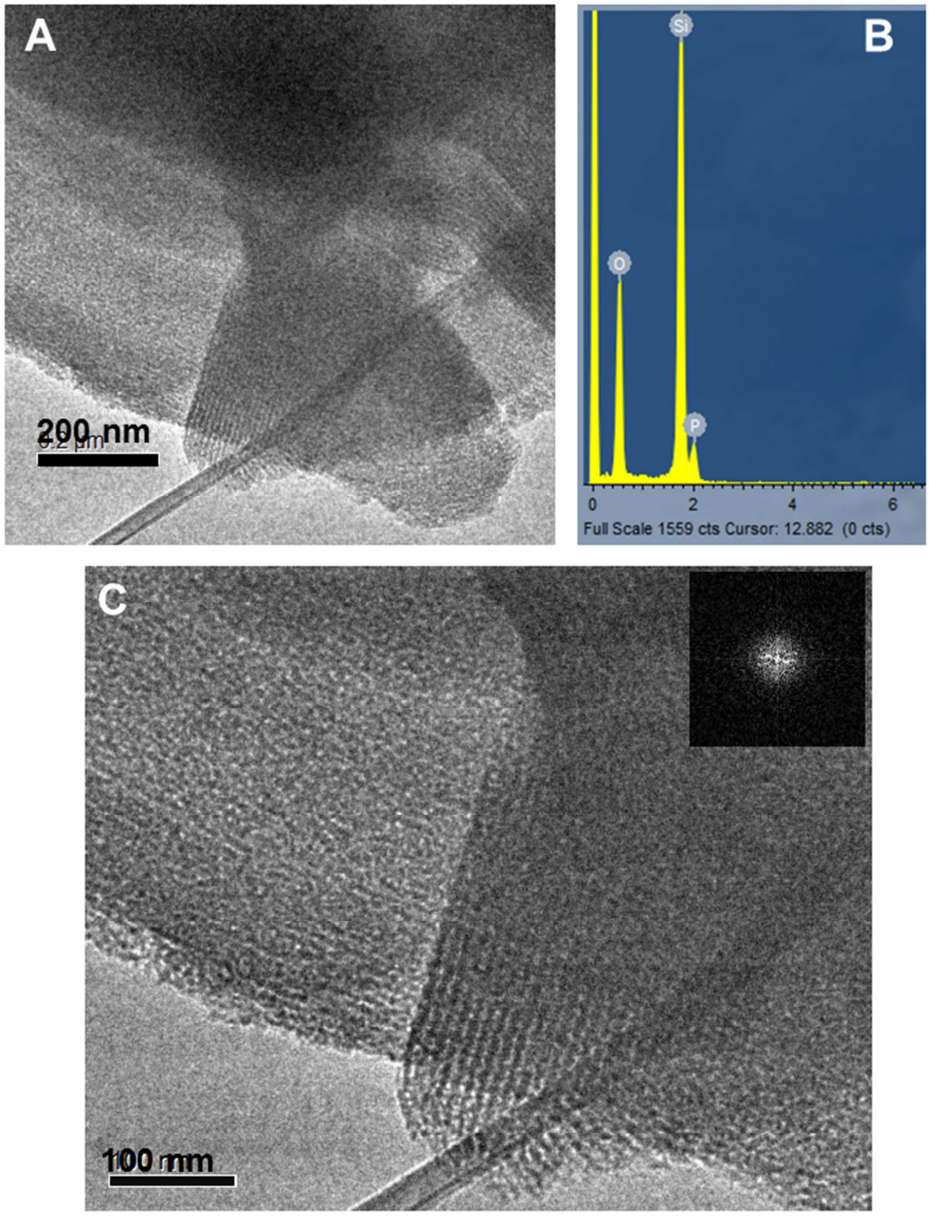
A
200 nm
B
Si
O
P
0
2
4
6
Full Scale 1559 cts Cursor: 12.882 (0 cts)
C
100 nm

Figure 9

Highlights

1. Treating $SBA15_{DPT}$ with 12M HCl produces $-PO_3H_2$ groups but damages the mesostructure
2. HCl-$SBA15_{DPT}$ presents uncontrolled drug burst release compared with $SBA15_{DPT}$
3. XRD and N_2 adsorption are not enough to detect mesostructural damages in HCl-$SBA15_{DPT}$
4. HRTEM is essential to understand drug release from mesoporous materials